 https://doi.org/10.3311/PPci.41637

Periodica Polytechnica Civil Engineering, 70(2), pp. 424–435, 2026

Investigation of the Failure Modes of Embedded Corrugated Shear Connections in Steel-concrete Composite Girders

Gábor Németh[1*], Nauzika Kovács[1]

[1] Department of Structural Engineering, Faculty of Civil Engineering, Budapest University of Technology and Economics, Műegyetem rkp. 3., H-1111 Budapest, Hungary
[*] Corresponding author, e-mail: nemeth.gabor@edu.bme.hu

Received: 17 July 2025, Accepted: 02 March 2026, Published online: 22 April 2026

Abstract

Composite girders with corrugated webs and embedded shear connections have been developed in bridge design practice, making structures more advantageous compared to conventional composite structures with flat web and headed studs. To understand the structural behavior and determine the influence of structural parameters on longitudinal shear resistance, experimental and numerical testing of embedded shear connectors is essential. An experimental program of 43 push-out tests on embedded specimens with trapezoidal steel profiles has been completed at the Budapest University of Technology and Economics. Current paper presents a detailed evaluation of the experimental results of the full-scale push-out test series, focusing on structural parameters causing concrete failure (trapezoidal profile geometry, embedding depth, shear connectors). To investigate the influence of structural parameters (number and geometry of cutouts) on the failure modes of the corrugated steel web, a numerical model is developed. The study aims to investigate how structural parameters of the embedded corrugated web influence its behavior and failure modes, with particular focus on avoiding non-visible steel deterioration through appropriate detailing. The objective is to identify structural parameters that lead to concrete deterioration, occurring only after significant crack propagation, so that failure becomes visible before it happens. Conclusions are drawn based on the results of experimental and numerical investigations.

Keywords

steel-concrete composite structures, corrugated web, embedded shear connector, experimental test, numerical analysis

1 Introduction

1.1 Literature review

Corrugated web steel-concrete composite bridges have been constructed since the 1980s due to their numerous advantages, such as lower self-weight and faster construction compared to concrete structures, and higher transverse stiffness and buckling resistance compared to flat web composite structures [1]. Over the long term, the corrugated web has proven to be an excellent structural solution, and further developments have led to additional benefits. By omitting the top and bottom steel flanges and embedding the corrugated web directly into the concrete slabs, further savings in steel material and welding can be achieved. Additionally, the embedded portion of the corrugated web also functions as a shear connector. Bridges with embedded corrugated web connections have been constructed in Japan, including the Hondani Bridge and the Kurobegawa Bridge [2].

The currently applicable Eurocode [3] provides design formulas only for the widely used headed stud connector, considering two failure modes: shear failure of the headed stud and crushing of the concrete at the base of the stud. It does not address embedded corrugated connections, nor even concrete dowel connectors. In 2018, the ECCS published a comprehensive review [4] on non-conventional shear connectors, which includes test results, comparative assessments, and analytical models, with concrete dowels playing a central role.

Concrete dowels with open cutouts exhibit four primary failure modes under static loading [5–9]:

1. Concrete shearing occurs through bilateral shearing along the dowel interface and is decisive in cases of small openings combined with thick steel plates.
2. Concrete pry-out results from transversal tensile stresses, leading to a concrete cone fracture and it is decisive when dowels are placed too close to the concrete surface.

Cite this article as: Németh, G., Kovács, N. "Investigation of the Failure Modes of Embedded Corrugated Shear Connections in Steel-concrete Composite Girders", Periodica Polytechnica Civil Engineering, 70(2), pp. 424–435, 2026. https://doi.org/10.3311/PPci.41637

3. Vertical splitting may occur in beam-type sections with thin concrete elements, when splitting tensile forces exceed the tensile strength of the concrete, producing horizontal cracks at the height of the dowel.
4. Bending-shearing failure of steel leads to plastic failure of the steel dowel and becomes critical when steel thickness is low.

The first three failure modes are related to the concrete, while the fourth is governed by the steel. When using thin or weak steel in combination with strong concrete, failure tends to occur on the steel side; otherwise, concrete failure becomes decisive [10]. In the latter case, the amount and arrangement of reinforcement significantly influence the failure mechanism. Under cyclic loading, fatigue failure may also occur [7]. However, experimental results indicate that concrete fatigue failure can be ruled out as long as the maximum longitudinal shear force remains below 70% of the characteristic static capacity of the dowels [11].

For perfobond-type concrete dowels with closed cutouts, experimental studies have shown that the decisive failure mode is a combination of concrete shearing and the dowel action of penetrating reinforcement [12, 13]. Design recommendations have also been proposed for the economical and efficient detailing of concrete dowels [14]. Push-out tests with embedded corrugated web connections, incorporating concrete dowels [15, 16] and headed studs [17–19] welded to the embedded portion of the corrugated web, have demonstrated that failure consistently occurs in the concrete. The failure is characterized by severe cracking and crushing of the concrete. Under out-of-plane bending, a gap between the concrete and the corrugated web can be observed, resulting from the opening in the concrete slab [20, 21]. For closed-cut concrete dowels placed on corrugated plates, structural detailing recommendations have been proposed regarding their geometric characteristics [22].

1.2 Objective of the study

An experimental program of a full-scale embedded corrugated push-out test series conducted at the Department of Structural Engineering is presented in Németh et al. [23]. Within the test program, both slab opening failure and concrete crushing failure modes were observed. During concrete crushing, among the potential concrete dowel failure modes, shearing was observed – pry-out and splitting failures could not develop due to the strong transverse reinforcement. Failures involving concrete crushing resulted in significantly higher load-bearing capacities. The tested specimens included reference setups without additional shear connectors, as well as specimens with open cutout concrete dowels or headed studs. In all cases, failure occurred in the concrete, however, in specimens with multiple open cutouts per plate field, failure of the steel dowel may become relevant. Therefore, one of the aims of the study is to investigate this potential failure mode.

Another aim is to analyze the structural behavior of embedded corrugated profiles without any additional shear connectors through a detailed evaluation of the experimental series [23], as well as to investigate the behavior of concrete dowels where, in addition to the trapezoidal profile, penetrating reinforcement is used as shear connection. Furthermore, the study seeks to determine the effect of changes in key structural parameters on load-bearing capacity, and to identify the factors that have the greatest influence on shear resistance and failure mode.

2 Evaluation of concrete failure through push-out tests

The influence of the following parameters on the concrete failure is investigated by comparing the results of the push-out experimental program: geometry of the trapezoidal profile (inclination angle, plate field width), embedding depth, presence and geometry of concrete dowels. The resistance of each specimen is evaluated and the effect of the parameters is presented by the increasing/decreasing of the resistance comparing to the chosen reference specimen.

2.1 Experimental program and specimens

The specimens of the experimental program had different geometries and materials. Current study only details the evaluated 26 specimens, but properties for all specimens can be found in Németh et al. [23]. Five corrugated profile geometries (Fig. 1) were tested with different inclination angles and plate widths: Profile 'A' 30°, Profile 'B' 45° and Profile 'C' 60° with plate width of 200 mm; Profile 'D' 30° and Profile 'E' 45° with plate width of 100 mm. The geometry of the profile influenced the size of the specimens, since 200 mm plate width specimens were manufactured with one and a half, 100 mm plate width specimens were manufactured with two wavelengths of the profile, as Fig. 2 shows.

Reference specimens with no additional shear connectors and specimens with open cutout concrete dowels and penetrating rebars are evaluated. Three dowel types were investigated: CD1 short, CD2 long and CD3 double short, all of them with a ∅14 mm penetrating rebar; the geometry of concrete dowels is presented in Fig. 1.

The format of the specimen codes is illustrated with C-A1-C25-0: 'C': corrugated web, 'A': profile geometry, '1': # of specimen in the same set, 'C25': concrete strength,

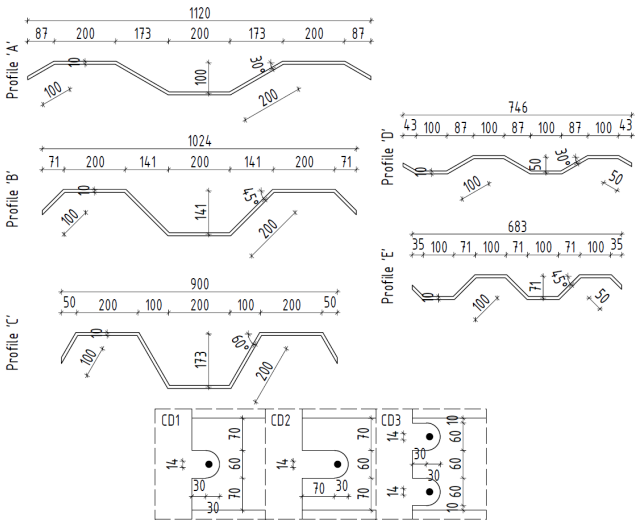

Fig. 1 Geometry of corrugated profiles and concrete dowels

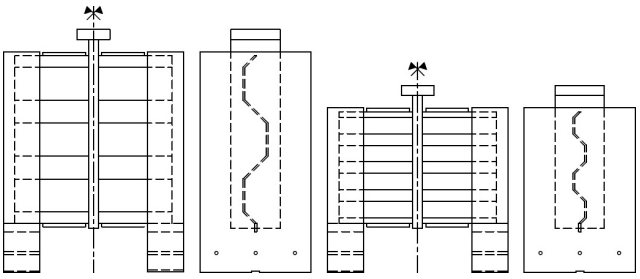

Fig. 2 Influence of profile geometry on global specimen geometry

'0': diameter of penetrating rebar [mm] (0 means reference specimen). Fig. 3 shows the two failure modes of the tests: slab opening due to transversal tension forces and concrete crushing under compression.

2.2 Methodology of test result evaluation

Force-displacement diagrams present the global displacement measured during the tests. No significant difference is observed in the initial stiffness or in the overall shape of the curves prior to reaching the ultimate load, although the curves show varying degrees of resistance degradation. Sudden jumps in the diagrams indicate signs of penetrating rebar failure. Diagrams are provided in Section 2.3, where all tested specimens are analyzed.

Fig. 3 Failure modes: slab opening and concrete crushing

A quantitative comparison is also conducted, and the results are summarized in tabular form. Each table (Tables 1 to 7) has the same layout, introducing the compared parameter(s) (e.g., inclination angle (α), plate width (a_1), embedding depth (t_E), concrete dowel (CD)); the ultimate longitudinal shear resistance measured during the test (P_{test}); resistance increasing effect of the examined parameters (Δ_{test}) is calculated by Eq. (1):

$$\Delta_{test} = \left(\frac{P_{test,comp}}{P_{test,base}} - 1 \right) \cdot 100\%, \tag{1}$$

where $P_{test,comp}$ is the shear capacity of the currently examined specimen (specimen to be compared), $P_{test,base}$ is the shear capacity of the reference specimen.

The value in the Δ_{test} column is calculated as $P_{test,comp}$ is the shear capacity of the given specimen, and $P_{test,base}$ is the shear capacity of the nearest 'base' specimen listed above. A 'base' label in the Δ_{test} column indicates that the specimens listed below are compared to this specimen until the next 'base' label appears. Positive values indicate an increase, while negative values indicate a decrease in shear capacity. It should be noted that not all possible specimen pairs are compared; only a representative selection is included to clearly demonstrate the trends. Nevertheless, the omitted comparisons are also taken into account when calculating the average change in load capacity.

Where the area compressed by the corrugated profile changes due to the compared parameters, the area of compressed-sheared surfaces per unit length (a_{comp}) is provided, calculated by Eq. (2):

$$a_{comp} = \frac{a_3 \cdot t_E}{L_{hw}}, \tag{2}$$

where a_3 is the projection of the inclined plate width perpendicular to the longitudinal axis, L_{hw} is the length of a half wave of the corrugation (see Fig. 4).

The experimental results are compared in Section 2.6 with the values calculated using the formulas presented below. The shear resistance of the connection was calculated as the sum of the shear resistance of compressed-sheared

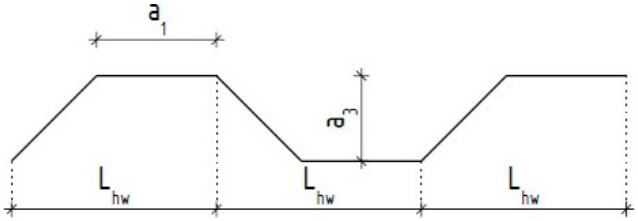

Fig. 4 Notation of geometric parameters

concrete blocks under the inclined fields (P_{emb}) and concrete dowels placed on the parallel fields (P_{dow}), normalized to a half wavelength, according to Eq. (3):

$$P_{calc} = \frac{P_{emb} + P_{dow}}{L_{hw}}. \tag{3}$$

For embedded corrugated connections, the following Eq. (4) estimate based on Japanese practice can be used for the shear resistance [19]:

$$P_{emb} = \frac{3}{5} f_{ck} \cdot a_3 \cdot t_E, \tag{4}$$

where f_{ck} is the compressive cylinder strength of concrete.

Several proposals exist for estimating concrete dowel resistance; one of the most accurate [13] is the formula proposed by Chen and Limazie [14], given in Eq. (5):

$$P_{dow} = 1.2 f_{cu} \cdot h_d \cdot t_w + 2.1 f_{ct} \cdot h_d \cdot t_w \left(1 + 13.5 \frac{E_s \cdot A_r}{E_{cm} \cdot h_d \cdot t_w}\right), \tag{5}$$

where f_{cu} is the compressive cube strength of concrete, h_d is the dowel height, t_w is the web thickness, f_{ct} is the tensile strength of concrete, E_s is the modulus of elasticity of steel, E_{cm} is the secant modulus of elasticity of concrete and A_r is the cross-sectional area of penetrating rebar.

2.3 Effect of inclination angle

Figs. 5 to 7 present the load-displacement curves of the specimens. The effect of inclination angle can be examined by comparing corrugated profiles A–B–C (30°, 45°, 60°) and D–E (30°, 45°). Fig. 5 presents load-displacement curves of the reference specimens (no penetrating rebars used), Figs. 6 and 7 show the curves for specimens with concrete dowels containing 14 mm diameter penetrating rebars.

The failure mode (Fig. 3) can be inferred from the shape of the curve: in the case of flatter curves, no concrete crushing is observed at failure load – the flatter the curve,

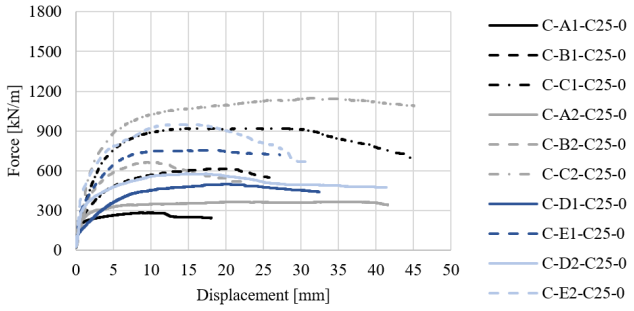

Fig. 5 Load-displacement curves of reference specimens – no concrete dowels (continuous: $\alpha = 30°$, dashed: $\alpha = 45°$, dashed dot: $\alpha = 60°$)

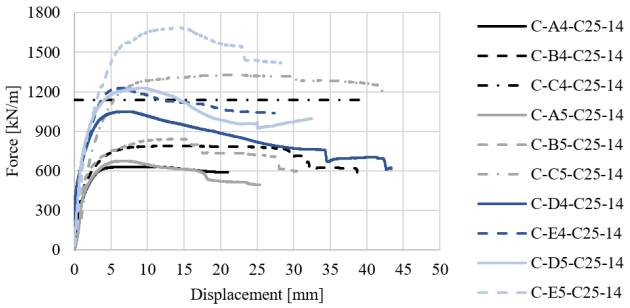

Fig. 6 Load-displacement curves of specimens with CD1 concrete dowels (continuous: $\alpha = 30°$, dashed: $\alpha = 45°$, dashed dot: $\alpha = 60°$)

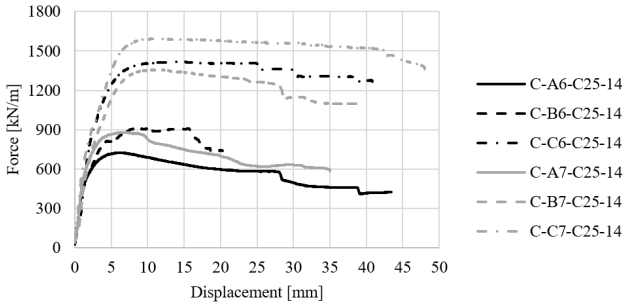

Fig. 7 Load-displacement curves of specimens with CD2–CD3 concrete dowels (continuous: $\alpha = 30°$, dashed: $\alpha = 45°$, dashed dot: $\alpha = 60°$)

the more dominant the role of slab opening becomes, resulting in lower resistance. In contrast, a shorter plateau and stronger degradation indicate a greater extent of concrete crushing, leading to higher resistance (compared to the respective reference specimen).

According to the test results, the inclination angle significantly increases the ultimate shear capacity. For reference specimens (Table 1) with a 200 mm plate width, the capacity increased by 82–117% from 30° to 45°, by 214–224% from 30° to 60°, and by 50–72% from 45° to 60°. For a 100 mm plate width, the increase was 52–65% from 30° to 45°. In the case of specimens with concrete dowels (Table 2), the corresponding increases for 200 mm plates were 25–55%, 80–97%, and 44–58%, respectively; while for 100 mm plates, the increase from 30° to 45° was 17–37%.

The observed increase in shear capacity with higher inclination angles can be attributed to the growing area of compressed-sheared concrete, as reflected by the values of a_{comp}. A higher inclination angle results in a larger concrete surface contributing to shear resistance, which explains the significant capacity gains in reference specimens. In contrast, in specimens with concrete dowels, the inclination angle has a much smaller effect on shear capacity. This is due to the role of the penetrating reinforcement, which holds the concrete slab together and limits its opening. By preventing the separation of the concrete,

Table 1 Test results of reference specimens for comparing the effect of inclination angle of the trapezoidal profile

Specimen	α (degree)	a_1 (mm)	P_{test} (kN/m)	Δ_{test} (α)		a_{comp} (cm^2/m)
C-A1-C25-0	30°	200	283	Base		2.7
C-B1-C25-0	45°	200	614	117%	Base	4.1
C-C1-C25-0	60°	200	918	224%	50%	5.8
C-A2-C25-0	30°	200	366	Base		4.0
C-B2-C25-0	45°	200	666	82%	Base	6.2
C-C2-C25-0	60°	200	1147	214%	72%	8.7
C-D1-C25-0	30°	100	498	Base		2.70
C-E1-C25-0	45°	100	755	52%		4.1
C-D2-C25-0	30°	100	577	Base		4.0
C-E2-C25-0	45°	100	950	65%		6.2

Alternating grey and white backgrounds indicate groups of comparable specimens.

Table 2 Test results of specimens with concrete dowels for comparing the effect of inclination angle of the trapezoidal profile

Specimen	α (degree)	a_1 (mm)	P_{test} (kN/m)	Δ_{test} (α)		a_{comp} (cm^2/m)
C-A4-C25-14	30°	200	631	Base		2.7
C-B4-C25-14	45°	200	789	25%	Base	4.1
C-C4-C25-14	60°	200	1137	80%	44%	5.8
C-A5-C25-14	30°	200	675	Base		4.0
C-B5-C25-14	45°	200	843	25%	Base	6.2
C-C5-C25-14	60°	200	1329	97%	58%	8.7
C-A6-C25-14	30°	200	725	Base		4.0
C-B6-C25-14	45°	200	911	26%	Base	6.2
C-C6-C25-14	60°	200	1415	95%	55%	8.7
C-A7-C25-14	30°	200	879	Base		4.0
C-B7-C25-14	45°	200	1358	55%	Base	6.2
C-C7-C25-14	60°	200	1594	81%	17%	8.7
C-D4-C25-14	30°	100	1050	Base		2.7
C-E4-C25-14	45°	100	1228	17%		4.1
C-D5-C25-14	30°	100	1229	Base		4.0
C-E5-C25-14	45°	100	1689	37%		6.2

Alternating grey and white backgrounds indicate groups of comparable specimens.

the penetrating rebars allow the corrugated steel web to maintain proper contact even at smaller inclination angles. As a result, increasing the inclination in these specimens adds relatively little to the load-bearing capacity compared to the reference specimens, where the slab can open freely.

Furthermore, the inclination angle influences the failure mode, especially in reference specimens, as Fig. 8 shows. At smaller angles, the horizontal component of the internal force (H) is more dominant, leading to failure by slab opening. At larger angles, the vertical force component (V) is more dominant, resulting in concrete crushing as the primary failure mode.

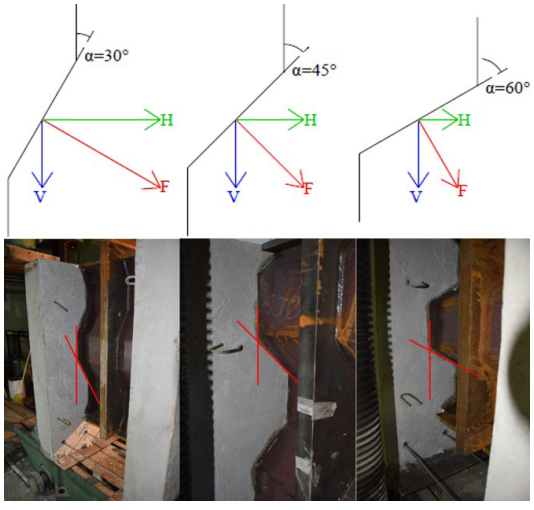

(a) (b) (c)

Fig. 8 Force components due to different inclination angles: (a) α = 30°; (b) α = 45°; (c) α = 60°

2.4 Effect of plate field width

The effect of plate width can be examined by comparing corrugated profiles A–D (200 mm, 100 mm) and

B–E (200 mm, 100 mm). According to the test results, reducing the plate width from 200 mm to 100 mm increased the shear resistance by 23–76% in reference specimens (Table 3) and by 56–101% in specimens with concrete dowels (Table 4).

In the case of smaller plate widths, the loaded concrete area remains the same (as indicated in the a_{comp} column). The higher shear capacity can be explained by the geometric interaction: as the two breakpoints of the inclined plate fields move closer together, these inclined fields are increasingly stiffened by the adjacent parallel plate segments. This stiffening effect enables the inclined plates to transfer more load onto the concrete, resulting in a more uniform stress distribution beneath them and, consequently, a higher load-bearing capacity.

2.5 Effect of embedding depth

The effect of embedding depth can be examined by comparing corrugated profiles number X1 (t_E = 100 mm) and number X2 (t_E = 150 mm) for the reference specimens, where X = A, B, C, D or E. For specimens with concrete dowels, profiles number X4 (t_E = 100 mm) and number X5 (t_E = 150 mm) can be compared.

According to the test results, increasing the embedding depth from 100 mm to 150 mm increased the shear resistance by 8–29% in reference specimens (Table 5) and by 7–38% in specimens with concrete dowels (Table 6)..

The increase in shear capacity with greater embedding depth is primarily due to the growth of the compressed-sheared concrete area, as reflected in the a_{comp} values. Although increasing the embedding depth from 100 mm to 150 mm enlarges the projected load transfer surface by 50%, the resulting capacity gain is more modest. This difference is explained by the uneven stress distribution along the embedded depth: shear deformations in the unembedded web lead to greater interaction near the steel-concrete interface, while the parts of the profile further from the web are less engaged, reducing the effectiveness of the additional surface.

The effect of increased embedding depth is also less pronounced at smaller inclination angles, where the dominant failure mode is slab opening. In such cases, the additional load-bearing surface contributes less to overall capacity. It should also be noted that in the case of specimen C-A1-C25-0, the test setup allowed for some bending moment absorption, resulting in lower measured capacity and a larger difference between specimens A1 and A2.

2.6 Effect of concrete dowels

The effect of concrete dowels on the embedded web was studied by comparing trapezoidal profiles number X2 (reference) with numbers X5, X6, and X7 (X = A, B, C, D or E), including short (CD1), long (CD2), and double short (CD3) dowels, respectively.

Table 3 Test results of reference specimens for comparing the effect of plate width of the trapezoidal profile

Specimen	α (degree)	a_1 (mm)	P_{test} (kN/m)	Δ_{test} (a_1)	a_{comp} (cm^2/m)
C-A1-C25-0	30°	200	283	Base	2.7
C-D1-C25-0	30°	100	498	76%	2.7
C-B1-C25-0	45°	200	614	Base	4.1
C-E1-C25-0	45°	100	755	23%	4.1
C-A2-C25-0	30°	200	366	Base	4.0
C-D2-C25-0	30°	100	577	58%	4.0
C-B2-C25-0	45°	200	666	Base	6.2
C-E2-C25-0	45°	100	950	43%	6.2

Alternating grey and white backgrounds indicate groups of comparable specimens.

Table 4 Test results of specimens with concrete dowels for comparing the effect of plate width of the trapezoidal profile

Specimen	α (degree)	a_1 (mm)	P_{test} (kN/m)	Δ_{test} (a_1)	a_{comp} (cm^2/m)
C-A4-C25-14	30°	200	631	Base	2.7
C-D4-C25-14	30°	100	1050	66%	2.7
C-B4-C25-14	45°	200	789	Base	4.1
C-E4-C25-14	45°	100	1228	56%	4.1
C-A5-C25-14	30°	200	675	Base	4.0
C-D5-C25-14	30°	100	1229	82%	4.0
C-B5-C25-14	45°	200	843	Base	6.2
C-E5-C25-14	45°	100	1689	101%	6.2

Alternating grey and white backgrounds indicate groups of comparable specimens.

Table 5 Test results of reference specimens comparing the effect of embedding depth of the trapezoidal profile

Specimen	t_E (mm)	α (degree)	P_{test} (kN/m)	Δ_{test} (t_E)	a_{comp} (cm^2/m)
C-A1-C25-0	100	30°	283	Base	2.7
C-A2-C25-0	150	30°	366	29%	4.0
C-B1-C25-0	100	45°	614	Base	4.1
C-B2-C25-0	150	45°	666	8%	6.2
C-C1-C25-0	100	60°	918	Base	5.8
C-C2-C25-0	150	60°	1147	25%	8.7
C-D1-C25-0	100	30°	498	Base	2.7
C-D2-C25-0	150	30°	577	16%	4.0
C-E1-C25-0	100	45°	755	Base	4.1
C-E2-C25-0	150	45°	950	26%	6.2

Alternating grey and white backgrounds indicate groups of comparable specimens.

Table 6 Test results of specimens with concrete dowels comparing the effect of embedding depth of the trapezoidal profile

Specimen	t_E (mm)	α (degree)	P_{test} (kN/m)	Δ_{test} (t_E)	a_{comp} (cm^2/m)
C-A4-C25-14	100	30°	631	Base	2.7
C-A5-C25-14	150	30°	675	7%	4.0
C-B4-C25-14	100	45°	789	Base	4.1
C-B5-C25-14	150	45°	843	7%	6.2
C-C4-C25-14	100	60°	1137	Base	5.8
C-C5-C25-14	150	60°	1329	17%	8.7
C-D4-C25-14	100	30°	1050	Base	2.7
C-D5-C25-14	150	30°	1229	17%	4.0
C-E4-C25-14	100	45°	1228	Base	4.1
C-E5-C25-14	150	45°	1689	38%	6.2

Alternating grey and white backgrounds indicate groups of comparable specimens.

Test specimens with the same plate width should be compared, as concrete dowels contribute more to shear resistance at smaller plate widths due to the higher number of connectors per unit length. Fig. 9 illustrates the effect of the number of concrete dowels through post-failure images: in Fig. 9 (a), a specimen with three dowels is shown, while Fig. 9 (b) presents a specimen with four dowels. The increased number of dowels results in a more uniform stress distribution, as shown by the more extensive cracking and crushing of the concrete observed in Fig. 9 (b).

(a) (b)

Fig. 9 Specimens with concrete dowels: (a) 3 dowels on a longer web in case of 200 mm plate width; (b) 4 dowels on a shorter web in case of 100 mm plate width

Table 7 presents the results of the examined specimens. According to the test series, short dowels (CD1) increased the ultimate shear capacity by approximately 16–123%, long dowels (CD2) by 23–98%, and double short dowels (CD3) by 39–140%.

The test results show a clear difference between specimens with 200 mm and 100 mm plate widths. As expected, a shorter plate width results in a more significant increase in load capacity due to the higher number of shear connectors per unit length.

Additional shear connectors not only enhance shear capacity but also influence the failure mode. However, their effectiveness reduces with increasing inclination angle (profiles A → B → C). As detailed in Section 2.3, this is because the horizontal force component – carried by the penetrating rebars – decreases as the inclination angle increases, reducing the absolute contribution of the connectors.

Comparing profiles A, B, and C (which include all dowel configurations), double short dowels (CD3) yield

Table 7 Test results of specimens for comparing the effect of concrete dowels

Specimen	CD	P_{test} (kN/m)	Δ_{test} (CD)		Δ_{test} (CD) (kN/m)	P_{calc} (kN/m)	Δ_{calc}
C-A2-C25-0	–	366	Base		Base	1041	185%
C-A5-C25-14	CD1	675	85%	Base	309	1156	71%
C-A6-C25-14	CD2	725	98%	7%	359	1214	67%
C-A7-C25-14	CD3	879	140%	30%	513	1414	61%
C-B2-C25-0	–	666	Base		Base	1555	134%
C-B5-C25-14	CD1	843	27%	Base	177	1915	127%
C-B6-C25-14	CD2	911	37%	8%	246	2053	125%
C-B7-C25-14	CD3	1358	104%	61%	692	1979	46%
C-C2-C25-0	–	1147	Base		Base	2168	89%
C-C5-C25-14	CD1	1329	16%	Base	182	2577	94%
C-C6-C25-14	CD2	1415	23%	7%	268	2749	94%
C-C7-C25-14	CD3	1594	39%	20%	447	2591	63%
C-D2-C25-0	–	577	Base		Base	1006	74%
C-D5-C25-14	CD1	1229	113%		652	1664	35%
C-E2-C25-0	–	950	Base		Base	1610	70%
C-E5-C25-14	CD1	1689	78%		740	2274	35%
C-A1-C25-0	–	283	Base		Base	543	92%
C-A4-C25-14	CD1	631	123%		348	890	41%
C-B1-C25-0	–	614	Base		Base	906	47%
C-B4-C25-14	CD1	789	29%		175	1217	53%
C-C1-C25-0	–	918	Base		Base	1262	37%
C-C4-C25-14	CD1	1137	24%		219	1599	41%
C-D1-C25-0	–	498	Base		Base	586	18%
C-D4-C25-14	CD1	1050	111%		551	1167	11%
C-E1-C25-0	–	755	Base		Base	906	20%
C-E4-C25-14	CD1	1228	63%		473	1534	25%

Alternating grey and white backgrounds indicate groups of comparable specimens.

the highest increase in shear capacity, followed by long dowels (CD2), and then short dowels (CD1), as expected. On average, CD3 dowels provide an additional 328 kN/m (or 37.1%) shear capacity compared to CD1 dowels. The expected trend – namely that the capacity increase from CD3 dowels is approximately double that of CD1 – is roughly confirmed by the test series.

The results calculated using Eq. (3), along with their difference from the measured values, are shown in the P_{calc} and Δ_{calc} columns. The formula consistently overestimates the resistance; however, significant differences are observed for most reference specimens (X1 and X2, X = A, B, C, D or E). This can be attributed to the failure mode being slab opening rather than concrete crushing. For a given profile, the most accurate results were obtained for specimens with CD3 dowels (X7), likely because the formulas were developed for evenly spaced, closely arranged dowels over one wavelength – a condition better approximated in double-dowel configurations. For the same reason, the best agreement is found in 100 mm plate width specimens with dowels (Y4 and Y5, Y = D or E), where the dowels are most densely spaced relative to the profile.

3 Evaluation of steel failure through numerical analysis

A numerical model was developed to complement the experimental results, which resulted only in concrete failure modes. The FE model was calibrated by material test results, then the geometry of the corrugated steel profile was modified to investigate the structural behavior of the steel component of the connection. The following parameters were investigated: number, height and spacing of dowels.

3.1 Introduction of numerical model

In the numerical analysis, the aim was to examine the influence of the geometry of the steel block between concrete dowels. For this purpose, simulations were performed using geometry type 'B' (see Fig. 1). The height of the trapezoidal plate is 450 mm, embedded into the concrete slab to a depth of 150 mm from the top edge.

The concrete dowel connectors (Fig. 10) were modelled as cutouts on the plate fields parallel to the longitudinal axis, located within the embedded region. The total length of short cutouts (CD1) is 60 mm, while long cutouts (CD2) measure 100 mm. One cutout and two cutouts (CD3, CD4) were applied per plate field. In the latter case, the steel block between the two cutouts typically measures 60 mm in width. Additionally, a modified version with double long cut-outs placed closer (30 mm) to each other (CD5) was introduced to analyze potential bending failure of the steel block between the cutouts.

The numerical model was developed in ABAQUS/Explicit [24] environment using C3D8R hexahedral elements. To avoid concrete failure, only elastic-plastic behavior was defined for the concrete. The steel-concrete interaction was modeled using contact interaction with normal behavior defined as "hard" formulation and tangential behavior as "penalty" friction formulation with a friction coefficient of 0.40. The material model for steel was calibrated based on the results of tensile coupon tests, following the procedure of Pavlović et al. [25]. In addition to elastic and plastic behavior, ductile and shear damage initiation and evolution criteria were also defined. Fig. 11 presents the result of the material calibration. Fig. 12 shows the model with the applied boundary conditions and displacement loading. A mesh sensitivity analysis was carried out; the difference in ultimate load between the adopted mesh (15 mm) and a finer mesh (7.5 mm) was 2.4%, confirming sufficient accuracy.

For validation purposes, a numerical simulation of the push-out specimen C-B2-C25-0 was performed using a Concrete Damage Plasticity (CDP) model to represent concrete failure. The material parameters were defined

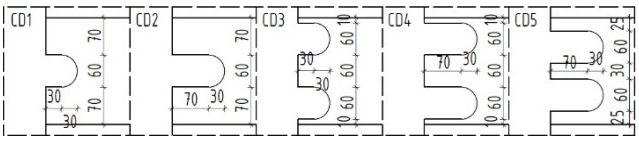

Fig. 10 Geometry of the concrete dowels

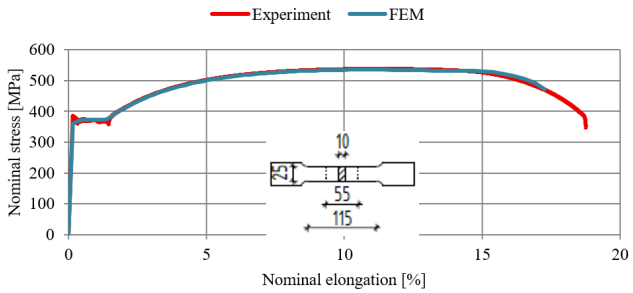

Fig. 11 Experimental and numerical tensile coupon tests results

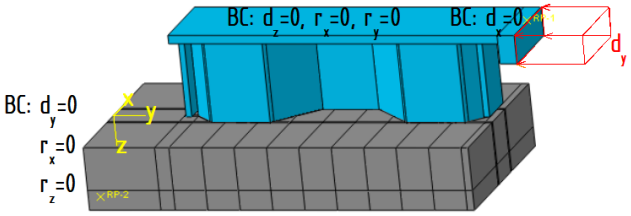

Fig. 12 Boundary conditions and displacement loading of the FE model

based on the measured compressive strength and values derived from Eurocode provisions. The plasticity parameters were adopted according to the literature recommendation [25]: $\varepsilon = 0.1$, $\sigma_{b0}/\sigma_{c0} = 1.16$, $\psi = 38°$ and $K_c = 2/3$. The reinforcement bars were modeled using T3D2 elements with a bilinear material model.

Fig. 13 shows the comparison of the experimental and numerical load-displacement curves. The predicted ultimate load differed by −0.32% from the experimental value. Good agreement was observed in both the initial stiffness and the post-peak response. The results confirm that the numerical model adequately reproduces the global structural behavior within the investigated scope.

3.2 Results and evaluation of numerical analysis

Fig. 14 shows the force-displacement curves from the numerical simulations investigating steel failure. For reference, the test result of the single short dowel (CD1) is also included in Fig. 14. The initial stiffness shows good

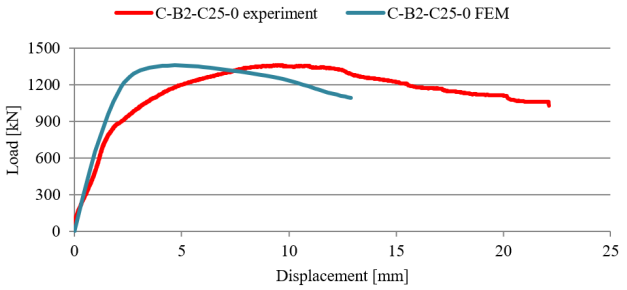

Fig. 13 Experimental and numerical load-displacement curves of C-B2-C25-0 specimen

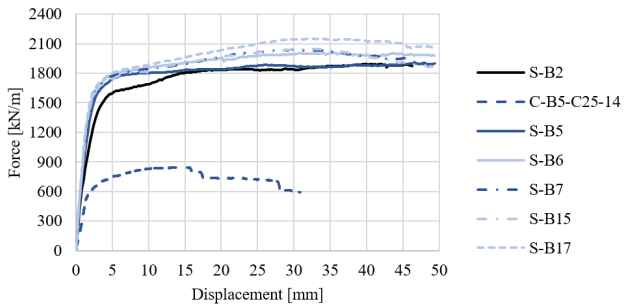

Fig. 14 Load-displacement curves of FE models (continuous: ref/single dowel (CD1, CD2), dashed dot: double dowel (CD3, CD4), dot: closely spaced double dowel (CD5), dashed: test result)

agreement with the model; beyond this, comparison is not relevant due to the differing failure modes. The models differ only in the dowel geometry, as defined in Table 8 (for dowel types, see Fig. 10). Table 8 summarizes the failure-specific load capacities of the steel (p_s) and concrete (p_c) components based on numerical and experimental results in relation to the number of cutouts and cutout length (l_{CD}).

Fig. 15 shows the stress distribution around the cutouts. Comparing the reference profile with those containing cutouts reveals that, while stresses in the reference profile concentrate near the inclined fields – mainly at the edges – plastic zones also develop around the cutouts in the dowel profiles. This indicates that the concrete transfers load through the dowels, distributing the force over a larger area compared to the reference specimens.

Unlike in the reference profile, the plate fields parallel to the longitudinal axis contribute to load-bearing when cutouts are present. Comparing single and double cutouts reveals that bending and shearing occur in the steel blocks between adjacent cutouts. When the cutouts are spaced far apart, bending of the plate between them is visible, but failure remains governed by material yielding near the profile corner. In contrast, closely spaced cutouts lead to a clear bending failure of the steel plate between them.

The steel web transfers the load to the concrete through the inclined plate fields. The bearing surface is slightly increased by the edges of the cutouts in the parallel plate fields, resulting in a modest increase in the steel-side resistance (1–6%). Similarly, doubling the number of cutouts leads to only a minor further increase in resistance (2–7%).

Comparing long cutouts placed at different distances, closer spacing results in higher load capacity. When cutouts are spaced farther apart, weakening occurs near the edges of the parallel plate fields, reducing the stiffening effect of the corner transitions and promoting early failure near the edges. In contrast, closer cutouts maintain this stiffening effect, leading to a bending-shear failure mode between the cutouts and thus increased resistance.

Table 8 Load capacities of steel and concrete part of shear connector

Specimen	CD	l_{CD} (mm)	p_s (kN/m)	p_c (kN/m)	$\Delta_{s\text{-}c}$
S-B2	–	–	1892	666	184%
S-B5	CD1	60	1902	843	126%
S-B7	CD3	60	2038	1358	50%
S-B6	CD2	100	2005	911	120%
S-B15	CD4	100	2051	–	–
S-B17	CD5	100	2153	–	–

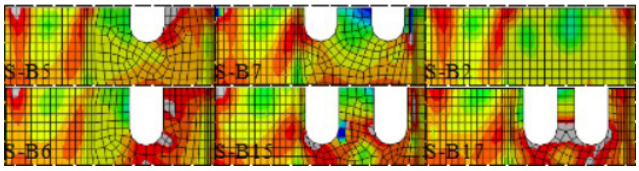

Fig. 15 Stresses around the cutouts

3.3 Detailing rules to prevent steel failure

Steel failure – yielding around the edge or shear-bending failure of steel dowels – should preferably be avoided to allow the concrete resistance to be fully utilized. To ensure this, based on the failure mechanisms identified in the numerical analysis, two simple detailing rules are recommended, shown on Fig. 16.

To ensure proper support of the inclined steel plates by the parallel fields, the distance from the cutout to the edge must be limited. Assuming a 45° stress propagation angle, the minimum edge-to-cutout distance can be calculated using Eq. (6) (for notations see Fig. 16):

$$b_{ed} \geq c_d + \frac{\sqrt{2}}{4} D_d. \tag{6}$$

To avoid shear failure of the steel dowel, its shear resistance must exceed that of the concrete dowel ($P_{st} \geq P_{dow}$). The shear resistance of the steel dowel [7] can be calculated using Eq. (7):

$$P_{st} = f_y \cdot b_s \cdot t_w, \tag{7}$$

where f_y is the yield strength of steel and b_s is the steel dowel width.

The recommended amount of penetrating rebar can be determined based on the ratio of concrete bearing capacity to steel yield strength [22]. The first term of Eq. (5) corresponds to the bearing capacity of the concrete dowel; thus, the recommendation can be expressed by Eq. (8):

$$A_r = \frac{1.2 f_{cu} \cdot h_d \cdot t_w}{f_s}, \tag{8}$$

where f_s is the yield strength of the rebar. Substituting Eq. (8) into Eq. (5) and equating it to Eq. (7), then solving for b_s, yields Eq. (9):

$$b_s = \frac{h_d}{f_y}\left(1.2 f_{cu} + 2.1 f_{ct}\left(1 + 13.5 \frac{E_s}{E_{cm}} \frac{1.2 f_{cu}}{f_s}\right)\right). \tag{9}$$

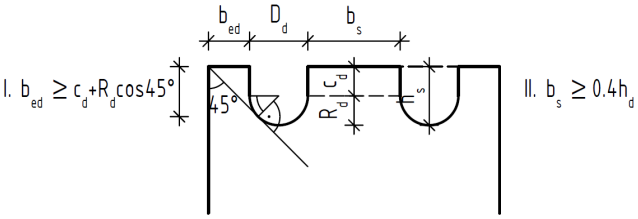

Fig. 16 Detailing rules and notations of dowel parameters

In the formula, only material properties remain besides h_d. Substituting typical material parameters used in bridge construction – S355 steel, C40/50 concrete and B500B reinforcement – yields Eq. (10):

$$b_s \geq 0.4 h_d. \tag{10}$$

Thus, a linear condition can be defined between the height of the concrete dowel and the width of the steel dowel, applicable under the use of the above materials and the penetrating rebar condition given in Eq. (8).

4 Conclusions

Based on the evaluation of push-out tests, the main conclusions regarding concrete failure are as follows:

1. Two failure modes were observed: slab opening at smaller inclination angles governed by horizontal force components, and concrete crushing at larger angles driven by vertical components.
2. Higher inclination angles increase shear capacity in reference specimens due to a larger compressed-sheared concrete area and by limiting slab opening. However, in specimens with concrete dowels, this effect is less pronounced, as the rebars limit slab opening and enable efficient load transfer even at smaller angles.
3. Smaller plate widths result in higher shear capacity, as the closer spacing of parallel plate fields stiffens the inclined fields better and leads to a more uniform stress distribution in the concrete.
4. Greater embedding depth increases the load-bearing surface, but the capacity gain is limited by uneven stress distribution along the depth – especially at smaller inclination angles, where slab opening remains the dominant failure mode.
5. Concrete dowels significantly enhance shear capacity and affect the failure mechanism. Their effectiveness decreases with increasing inclination angle.

Based on the evaluation of numerical models, the main conclusions regarding steel failure are as follows:

1. The presence of cutouts engages the parallel plate fields in load transfer.
2. When multiple cutouts are placed within the same plate field, bending and shearing of the steel blocks between concrete dowels can occur – especially when the cutouts are closely spaced, shifting the failure mode from edge yielding to local plate bending-shearing.
3. The stiffening effect of the profile corners is critical. Cutouts placed too close to the corners weaken the transition between parallel and inclined fields, promoting early plastic failure near the edges. In contrast, closer cutouts preserve edge stiffness and enable higher resistance through bending-shear action between the cutouts. To prevent steel failure, two detailing rules have been defined, ensuring that the structural response remains governed by externally observable concrete degradation.

The resistance formula based on concrete crushing, compiled from literature, was evaluated against experimental results. It overestimates the resistance and should be refined in future work based on the observations during evaluation. The proposed detailing rules correspond to the analyzed geometries and chosen material properties. Generalization for other geometries beyond the investigated dowel configuration needs further investigation.

Acknowledgement

The research program is part of the "BridgeBeam" R&D project No. GINOP-2.1.1-15-2015-00659, the financial support is gratefully acknowledged. Through the first author, the research was supported by the ÚNKP-19-3 New National Excellence Program of the Ministry for Innovation and Technology.

References

[1] Cheyrezy, M., Combault, J. "Composite Bridges with Corrugated Steel Webs - Achievements and Prospects", IABSE Reports, 60, pp. 479–484, 1990. https://doi.org/10.5169/SEALS-46526

[2] Ikeda, S., Sakurada, M. "Development of Hybrid Prestressed Concrete Bridges with Corrugated Steel Web Construction", presented at 30th Conference on Our World in Concrete & Structures, Singapore, Singapore, Aug 23-24, 2005.

[3] CEN "EN 1994-1-1: Eurocode 4: Design of Composite Steel and Concrete Structures – Part 1-1: General Rules and Rules for Buildings", European Committee for Standardization, Brussels, Belgium, 2004.

[4] Neves, L. C., Velasco, P. C., Valente, I. B. "Shear Connectors That Use Concrete Dowels", ECCS – European Convention for Constructional Steelwork, 2018. ISBN 978-92-9147-142-3

[5] Mangerig, I., Zapfe, C. "Concrete Dowels as Alternative Shear Connection", presented at 6th Japanese-German Bridge Symposium, Munich, Germany, Aug 29-Sep 1, 2005.

[6] Hauke, B. "Ductile Shear Connectors for High Strength Composite Members", presented at Fédération Internationale du Béton 2nd International Congress, Naples, Italy, Jun 5-8, 2006.

[7] Feldmann, M., Kopp, M., Pak, D. "Composite Dowels as Shear Connectors for Composite Beams – Background to the German Technical Approval", Steel Construction, 9(2), pp. 80–88, 2016. https://doi.org/10.1002/stco.201610020

[8] Classen, M., Hegger, J. "Shear-Slip Behaviour and Ductility of Composite Dowel Connectors with Pry-out Failure", Engineering Structures, 150, pp. 428–437, 2017. https://doi.org/10.1016/j.engstruct.2017.07.065

[9] Kopp, M., Wolters, K., Claßen, M., Hegger, J., Gündel, M., Gallwoszus, J., Heinemeyer, S., Feldmann, M. "Composite Dowels as Shear Connectors for Composite Beams – Background to the Design Concept for Static Loading", Journal of Constructional Steel Research, 147, pp. 488–503, 2018. https://doi.org/10.1016/j.jcsr.2018.04.013

[10] Seidl, G., Petzek, E., Băncilă, R. "Composite Dowels in Bridges - Efficient Solution", Advanced Materials Research, 814, pp. 193–206, 2013. https://doi.org/10.4028/www.scientific.net/AMR.814.193

[11] Lorenc, W. "Concrete Failure of Composite Dowels under Cyclic Loading during Full-Scale Tests of Beams for the "Wierna Rzeka" Bridge", Engineering Structures, 209, 110199, 2020. https://doi.org/10.1016/j.engstruct.2020.110199

[12] Ahn, J.-H., Lee, C.-G., Won, J.-H., Kim, S.-H. "Shear resistance of the perfobond-rib shear connector depending on concrete strength and rib arrangement", Journal of Constructional Steel Research, 66(10), pp. 1295–1307, 2010. https://doi.org/10.1016/j.jcsr.2010.04.008

[13] Aggelopoulos, E., Schorr, J., Kuhlmann, U. "Shear resistance of concrete dowels in composite slim-floor beams", ce/papers, 4(2–4), pp. 772–780, 2021. https://doi.org/10.1002/cepa.1360

[14] Chen, S., Limazie, T. "Composite Slim Floor Beams with Innovative Shear Connections", Proceedings of the Institution of Civil Engineers - Structures and Buildings, 171(1), pp. 29–37, 2018. https://doi.org/10.1680/jstbu.16.00171

[15] Novàk, B., Röhm, J. "Anwendung von Trapezblechstegen im Brückenbau: Längsschubtragverhalten von Betondübeln in Kombination mit Trapezblechstegen" (The use of corrugated steel webs in bridge constructions: Load bearing behaviour of concrete dowels in combination with corrugated steel webs under longitudinal shear), Beton- und Stahlbetonbau, 104(9), pp. 562–569, 2009. (in German) https://doi.org/10.1002/best.200900685

[16] Kim, S.-H., Ahn, J.-H., Choi, K.-T., Jung, C.-Y. "Experimental Evaluation of the Shear Resistance of Corrugated Perfobond Rib Shear Connections", Advances in Structural Engineering, 14(2), pp. 249–263, 2011. https://doi.org/10.1260/1369-4332.14.2.249

[17] Raichle, J., Kuhlmann, U. "Trapezblechstege im Verbundbau: Längsschub und Querbiegung der Verbundfuge mit randnahen Kopfbolzen" (Corrugated steel webs in composite construction: longitudinal shear and transverse bending moment with headed studs close to the concrete surface), Stahlbau, 84(10), pp. 763–770, 2015. (in German) https://doi.org/10.1002/stab.201510317

[18] Hu, F., Liu, X.-D., Yuan, Y.-G., Han, W.-S., Xu, X., Wang, J.-F. "波形钢腹板组合箱梁带栓钉埋入式抗剪连接件承载力推出试验及有限元模拟分析研究" (The capacity of embedded shear connector studs of composite box girders with a corrugated steel web by push-out tests and FEM analyses), Engineering Mechanics, 38(11), pp. 43–56, 2021. (in Chinese) https://doi.org/10.6052/j.issn.1000-4750.2020.09.0695

[19] Cheng, C., Wan, S., Song, A. "Experimental and numerical study on the mechanical properties of embedded double-row-pins connectors", Structures, 35, pp. 214–232, 2022. https://doi.org/10.1016/j.istruc.2021.11.006

[20] Kosa, K., Awane, S., Uchino, H., Fujibayashi, K. "埋込み接合方式を用いた波形鋼板ウェブ PC 橋の終局挙動に関する研究" (Ultimate Behavior of Prestressed Concrete Bridge with Corrugated Steel Webs Using Embedded Connection), JSCE Journal of Materials, Concrete Structures and Pavements, 62(1), pp. 202–220, 2006. https://doi.org/10.2208/jsceje.62.202

[21] Röhm, J., Novàk, B. "Querbiegetragverhalten von Betondübeln bei Verbundtragwerken mit Trapezblechstegen" (Behavior of Composite Structures with Corrugated Steel Webs under Transverse Bending using Dowels), Beton und Stahlbetonbau, 105(3), pp. 176–185, 2010. (in German) https://doi.org/10.1002/best.200900068

[22] Sayed-Ahmed, E.Y. "Concrete Dowels: Innovative Shear Connectors for Composite Girders with Corrugated Steel Webs", In: 9th Arab Structural engineering Conference Proceedings, Abu Dhabi, United Arab Emirates, 2003, pp. 73–80. ISBN 9948-02-099-5 [online] Available at: https://www.researchgate.net/publication/280609461_CONCRETE_DOWELS_INNOVATIVE_SHEAR_CONNECTORS_FOR_COMPOSITE_GIRDERS_WITH_CORRUGATED_STEEL_WEBS [Accessed: 16 July 2025]

[23] Németh, G., Jáger, B., Kövesdi, B., Kovács, N. "Experimental Investigation of Steel-Concrete Composite Push-Out Tests with Embedded Corrugated Web", Advances in Structural Engineering, 25(11), pp. 2332–2347, 2022. https://doi.org/10.1177/13694332221095627

[24] Dassault Systèmes "Abaqus/CAE (Version 6.14-5)", [computer program] Available at: https://www.3ds.com/products/simulia/abaqus/ [Accessed: 14 July 2025]

[25] Pavlović, M., Marković, Z., Veljković, M., Buđevac, D. "Bolted shear connectors vs. headed studs behaviour in push-out tests", Journal of Constructional Steel Research, 88, pp. 134–149, 2013. https://doi.org/10.1016/j.jcsr.2013.05.003